XAS: Theory

September 29, 2022

A running list of notes on the theory and practical calculation of x-ray absorption spectra (specifically XANES and EXAFS).

1 Theory Overview and notables

1.1 Notes from Global XAS Journal club Youtube videos

1.1.1 Computational X-ray Spectroscopy, Matching Peaks and Missing Features (John Vinson)

- X-rays (100 eV - 10 keV)
- Probes, specifically focusing on near-edge spectroscopy (XANES): absorption and emission
- Forward problem, inverse problem, BSE equation
- measuring an excited state (excitons, phonons, plasmons, magnons)
- computational approaches to map material -> ground-state -> X-ray response
- Forward problem: from structure to spectra?
  - included but wrong: critiques on DFT
  - neglected or simplified: thermal disorder, electron-phonon, many-body or multi-excitation terms
- Inverse problem: from spectra to structure?
  - accuracy of forward problem, non-uniqueness, open-ended problem
- BSE equation and OCEAN code

$$H_{BSE} = H_e - H_h + H_{eh}$$

$$H_e = -\frac{\nabla^2}{2} + V_{ion} + \int d^3r' \frac{\rho(\mathbf{r})}{|\mathbf{r} - \mathbf{r}'|} + V_{xc}[\rho(\mathbf{r})] + \Sigma \qquad \text{(DFT or DFT/GW)}$$

$$H_h = E_h - i\Gamma_j + \chi_j$$

H_{eh} has terms to lowest order: direct term (excitonic binding, screening), exchange (leads to L_3, L_2 mixing for transition metals)

- some systems lacking: electron-phonon coupling (e.g., nickel oxide); BSE assumes single electron-hole; not capture localized charge transfer thing
- Example case: spinel lithium titanate (battery anode candidate with small volume changes with lithiation but crappy conducivity and mobility of Li)
  - dope with Mn and figuring out where it goes in the lattice based on XAS: Ti site, Li site, or interstitial
  - first calculated and sorted by total energies
  - second simulated Mn K-edge
- Example case: redox in Li batteries- oxidation of oxygen in battery cathodes
  - where are electrons coming from
  - other possibilities
    - bond length- but issues if have disordered system
    - XAS: directly with O K-edge absorption or via elimination by looking at transition metals
    - XAS can be convoluted/misleaded; changing electron density changes the allowed transitions but also changes rest of screening behavior of the rest of system, so difficult to deconvolute
  - fingerprint with RIXS instead- what happens after the core-level hole is created; basically if the core-hole decays from VBM electron falling down leading to exciton formation
- something about the elastic line (excitations below excitonic things)
- accounting for thermal vibrations
  - create ensemble from MD; will mostly excite low-lying modes within kT
  - build structures from phonon modes, include $1/2 + n(\omega, t)$ quantum-phonon occupations; Vinson et al PRB 90, 205207 (2014); example of NH3NO molecule- including quantum phonon occupations accounts for missing peak found in 0K XAS but "missing" in experimental spectra
    - get lifetimes from GW- show that missing peak associated with NO σ is due to those states having large lifetime broadening (short lived)

1.2 Fundamentals of x-ray absorption fine structure Newville

- XAFS = XANES + EXAFS
- local atomic coordination, chemical/oxidation state; works at low concentrations, minimal sample prep
- X-ray absorption via photoelectric effect

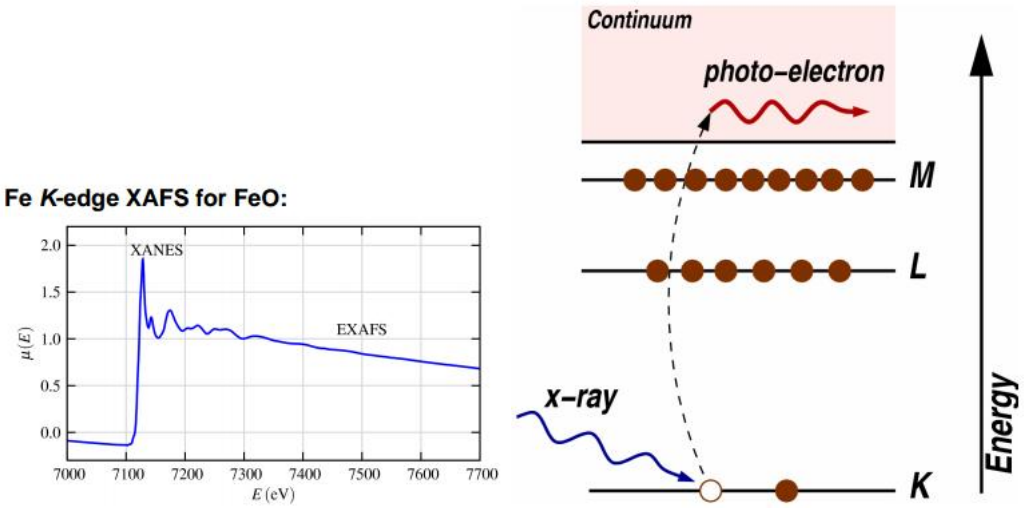

- secondary effects: x-ray fluorescence and Auger
- absorption coefficient $\mu = -d \ln I/dx \approx \frac{\rho Z^4}{AE^3}$ for density ρ, atomic number Z, and atomic mass A as a function of x-ray energy E; $I = I_0 e^{-\mu t}$
- all elements with Z>18 have K- or L-edge between 3 and 35 keV, which can be accessed at many synchrotron sources
- EXAFS from multiple scattering of photoelectron
- multiple scattering most important when scattering angle is > 150 degrees

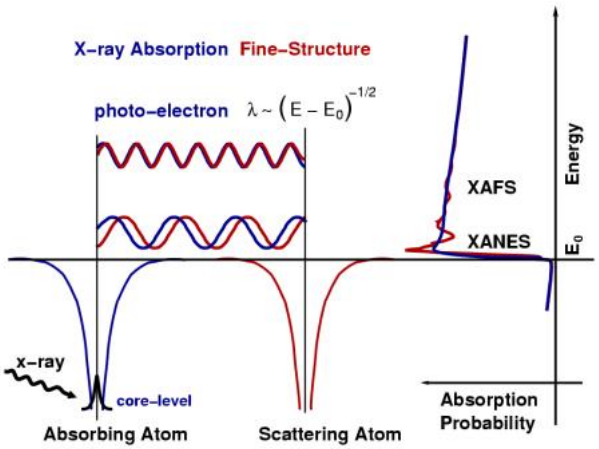

- $\chi(k[E]) = \frac{\mu(E)-\mu_0(E)}{\mu_0(E)}$

1.2.1 Procedure to process XANES data, using FeO as example

- convert intensities to $\mu(E) \rightarrow \mu(E)t = -\ln(I/I_0)$

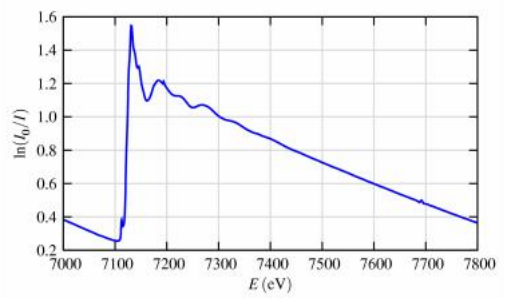

- subtract a smooth pre-edge function to remove instrumental background and absorption from other edges

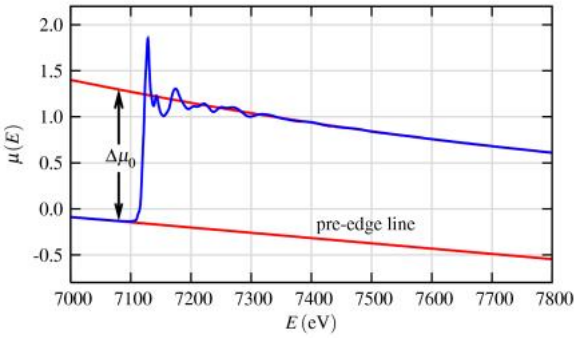

- normalize $\mu(E)$ to go from 0 to 1 to represent absorption of 1 x-ray; select edge step $\Delta\mu_0(E_0)$ by extrapolating a fit to $\mu(E)$ to this edge; select E_0as roughly the maximum of $d\mu/dE$

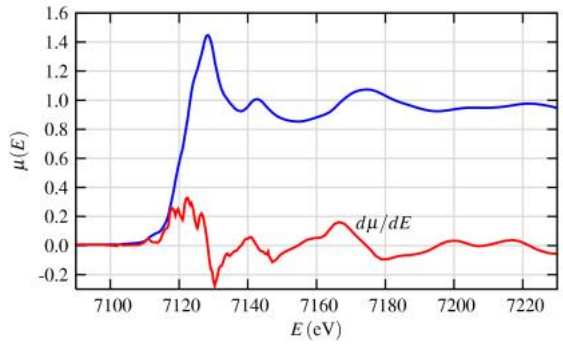

- remove smooth post-edge background to approximate $\mu_0(E)$ to obtain XAFS $\chi(E)$

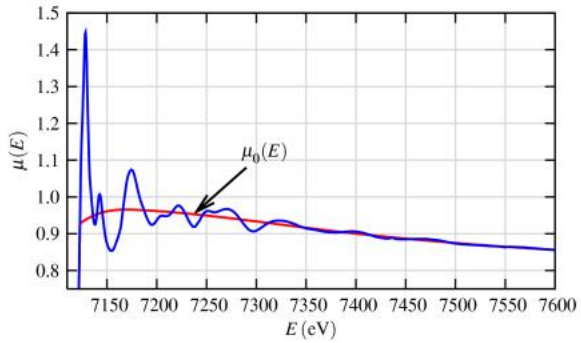

This can be somewhat dangerous – a flexible enough spline could match the $\mu(\mathbf{E})$ and remove all the EXAFS!

We want a spline that will match the *low frequency* components of $\mu_0(\mathbf{E})$.

- identify threshold energy $E_0 \rightarrow k = \sqrt{\frac{2m(E-E_0}{\hbar^2}}$; and convert to k, momentum of photoelectron
- weight $\chi(k)$ with k^2or $k^3$to amplify at large k; Fourier transform to real space

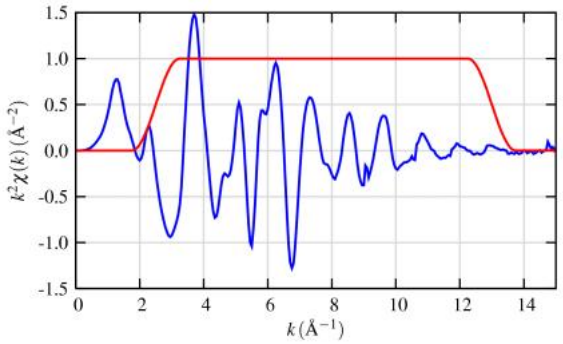

k-weighted $\chi(\mathbf{k})$: $\mathbf{k^2\chi(k)}$

$\chi(\mathbf{k})$ is composed of sine waves, so we'll Fourier Transform from $\mathbf{k}$ to $\mathbf{R}$-space. To avoid "ringing", we'll multiply by a *window function*.

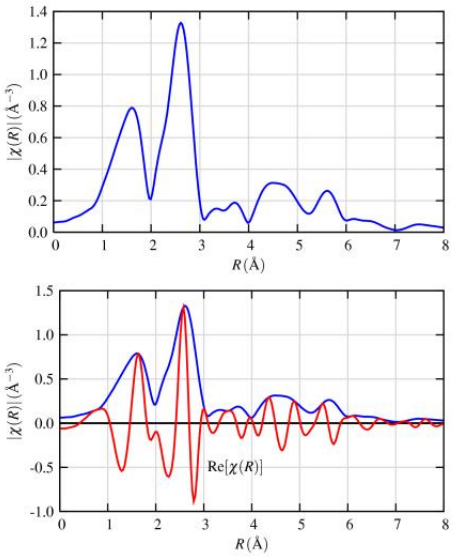

$\chi(\mathbf{R})$

The Fourier Transform of $\mathbf{k^2\chi(k)}$ has 2 main peaks, for the first 2 coordination shells: Fe-O and Fe-Fe.

The Fe-O distance in FeO is 2.14Å, but the first peak is at 1.6Å. This shift in the first peak is due to the *phase-shift*, $\boldsymbol{\delta}(\mathbf{k})$: $\sin[2\mathbf{kR} + \boldsymbol{\delta}(\mathbf{k})]$.

A shift of -0.5Å is typical.

$\chi(\mathbf{R})$ is complex:

The FT makes $\chi(\mathbf{R})$ complex. Usually only the amplitude is shown, but there are really oscillations in $\chi(\mathbf{R})$.

Both real and imaginary components are used in modeling.

- isolate $\chi(k)$ for individual "shell" via Fourier filtering

1.2.2 Procedure for EXAFS analysis, using FeO as example

FeO has a rock-salt structure.

To model the FeO EXAFS, we calculate the scattering amplitude $\mathbf{f(k)}$ and phase-shift $\boldsymbol{\delta}(\mathbf{k})$, based on a guess of the structure, with Fe-O distance $\mathbf{R} = 2.14$ Å (a regular octahedral coordination).

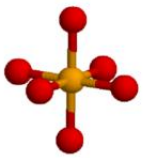

We'll use these functions to *refine* the values $\mathbf{R}$, $\mathbf{N}$, $\boldsymbol{\sigma}^2$, and $\mathbf{E_0}$ so our model EXAFS function matches our data.

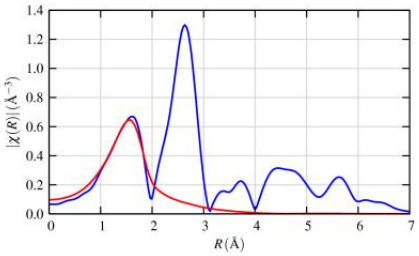

$|\chi(\mathbf{R})|$ for FeO (blue), and a 1st shell fit (red).

Fit results:

$\mathbf{N}$	= 5.8 ± 1.8
$\mathbf{R}$	= 2.10 ± 0.02Å
$\boldsymbol{\Delta E_0}$	= -3.1 ± 2.5 eV
$\boldsymbol{\sigma}^2$	= 0.015 ± 0.005 Å^2.

EXAFS Analysis: 1st Shell of FeO

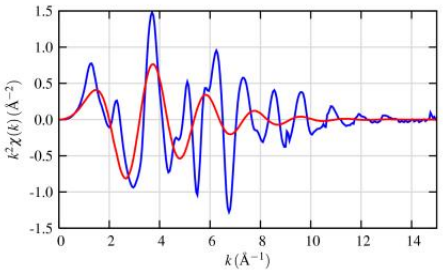

1st shell fit in k space.

The 1st shell fit to FeO in k space.

There is clearly another component in the XAFS!

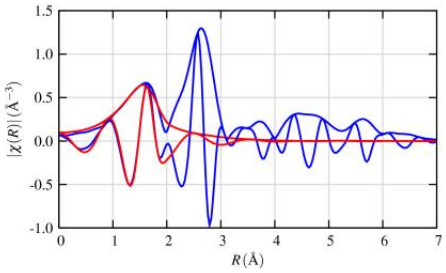

1st shell fit in R space.

$|\chi(R)|$ and Re$[\chi(R)]$ for FeO (blue), and a 1st shell fit (red).

Though the fit to the magnitude didn't look great, the fit to Re$[\chi(R)]$ looks very good.

EXAFS Analysis: Second Shell of FeO

To add the second shell Fe to the model, we use calculation for $f(k)$ and $\delta(k)$ based on a guess of the Fe-Fe distance, and refine the values R, N, σ^2.
Such a fit gives a result like this:

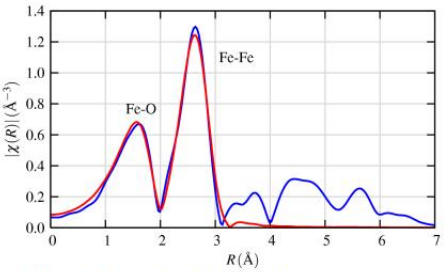

$|\chi(R)|$ data for FeO (blue), and fit of 1st and 2nd shells (red).
The results are fairly consistent with the known values for crystalline FeO:
6 O at 2.13Å, 12 Fe at 3.02Å.

Fit results (uncertainties in parentheses):

Shell	N	R (Å)	σ^2 (Å^2)	ΔE_0 (eV)
Fe-O	6.0(1.0)	2.10(.02)	0.015(.003)	-2.1(0.8)
Fe-Fe	11.7(1.3)	3.05(.02)	0.014(.002)	-2.1(0.8)

EXAFS Analysis: Second Shell of FeO

Other views of the data and two-shell fit:

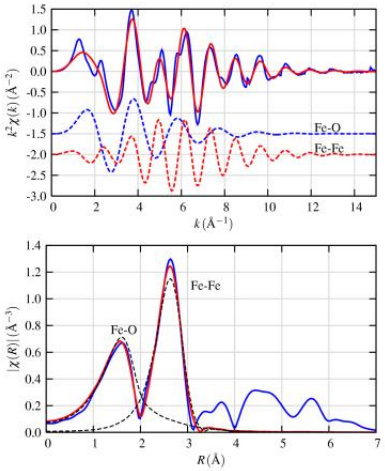

The Fe-Fe EXAFS extends to higher-k than the Fe-O EXAFS.

Even in this simple system, there is some *overlap* of shells in R-space.

The agreement in Re[χ(R)] look especially good – this is how the fits are done.

Of course, the modeling can get more complicated than this!

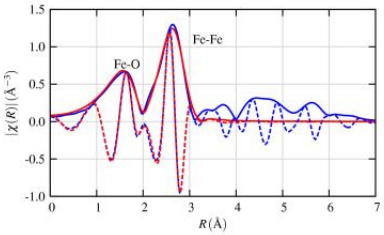

1.3 Theoretical approaches to x-ray absorption fine-structure (Rehr and Albers) 10.1103/RevModPhys.72.621

- absorption coefficient $\mu = -d \ln I/dx \approx \frac{\rho Z^4}{AE^3}$ for density ρ, atomic number Z, and atomic mass A as a function of x-ray energy E; $I = I_0 e^{-\mu t}$

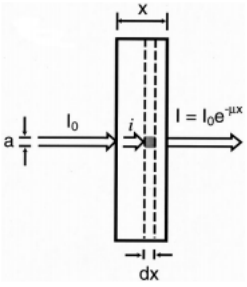

FIG. 1. Schematic view of x-ray absorption. I_0 is the intensity of the incoming x-ray beam, which has a cross-sectional dimension (width) a. Inside the slab of absorbing material (of total depth x), the intensity is i, and there is a loss of intensity dI in each infinitesimal slab of the material dx. After the x ray has traversed a distance x into the slab, the intensity has been reduced to $I = I_0 e^{-\mu x}$, where μ is the definition of the absorption coefficient. This figure was redrawn; it is based on Fig. I.1 of Müller (1980).

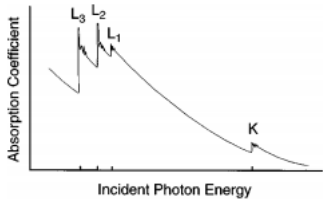

FIG. 2. Schematic view of x-ray absorption coefficient as a function of incident photon energy. Four x-ray edges are shown: K, L_1, L_2, and L_3. Note that the overall decrease in absorption as a function of energy is punctuated by four sharp, step-function-like increases at each edge. Above each edge are the oscillatory wiggles known as the EXAFS. This figure was redrawn; it is based on Fig. I.2 of Müller (1980).

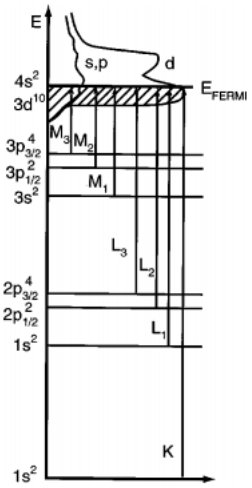

FIG. 3. The relationship between the x-ray absorption edges and the corresponding excitation of core electrons. Shown are the excitations corresponding to the K, L, and M x-ray absorption edges. The arrows show the threshold energy difference of each edge. Any transitions higher in energy (to unoccupied states above the Fermi energy E_F) are also allowed. This figure was redrawn; it is based on Fig. 1 of Grunes (1983).

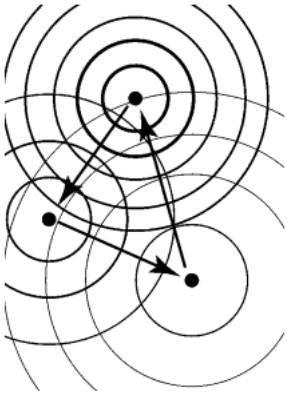

FIG. 5. Pictorial view of the multiple scattering of an outgoing wave off neighboring atoms. The topmost atom is the original source of the wave, which diffracts first off the atom at the lower left and finally off the atom at the lower right. Each successive outgoing spherical wave is weaker, which is reflected in the thickness of the spherical wave fronts. This type of path is called a triangular path.

- the main standard equation

$$\chi(k) = \sum_R S_0^2 N_R \frac{|f(k)|}{kR^2} \sin(2kR + 2\delta_c + \Phi) e^{-2R/\lambda(k)} e^{-2\sigma^2 k^2}$$

R= interatomic distances

N_R=coordination number (aka number of equivalent scatterers)

$f(k) = |f(k)|e^{i\Phi(k)}$ = the backscattering amplitude

Φ=quantum mechanical phase shift of backscattering; typically smaller than δ_c

δ_c= central-atom partial wave phase shift of the final state

$\lambda(k)$=energy-dependent XAFS mean free path; finite lifetime of wave and core-hole

S_0^2= overall amplitude factor $\in(0.7,1)$ due to many-body effects (e.g., core-hole presence); usually approx by constant

σ=temperature-dependent rms fluctuation of bond length; Debye-Waller factor $e^{-2\sigma^2 k^2}$; essential for EXAFS but not XANES (when $\sigma^2 k^2 \ll 1$)

$\sin(2kR)$ →captures wiggles in XAFS spectrum

- key approximations
  - Fermi's golden rule for absorption; choice of final state (i.e., with or without core-hole correction)
  - mufftin potential (when used with Green's function propagator)
  - curved wave or plane wave approximation

- scattering paths for densely packed fcc Cu

TABLE I. List of the first 20 most important multiple-scattering paths for fcc Cu. For each path, the table contains R_{eff} (one-half of the total path length), the relative mean path amplitude C_{cw} in percent (where the first path is arbitrarily assigned a value of 100%), the lengths of each leg using Lee and Pendry's notation (Lee and Pendry, 1975), the degeneracy of the path, the total number of legs in the path, and a brief description of the shape of the path. The mean path amplitude is an average of $|\chi(k)|$ over nine evenly spaced k points. This table is a partial reproduction of Table I of Zabinsky *et al.* (1995), where a more complete description is given. See also Fig. 18 for a pictorial representation of some of the paths.

Path	R_{eff}(Å)	C_{cw}(%)	Label	Degeneracy	Legs	Comment
1	2.56	100.00	11	12	2	ss, 1st shell
2	3.61	20.23	22	6	2	ss, 2nd shell
3	3.83	12.28	111	48	3	triangle
4	4.36	8.96	211	48	3	triangle
5	4.43	44.77	33	24	2	ss, 3rd shell
6	4.77	13.47	311	96	3	triangle
7	4.77	6.99	131	48	3	triangle
8	5.11	14.32	44	12	2	ss, 4th shell
9	5.11	32.63	411	24	3	shadow
10	5.11	7.17	141	12	3	linear
11	5.11	4.04	1111	48	4	dogleg
12	5.11	24.16	1111	12	4	shadow
13	5.11	8.74	1111	12	4	linear
14	5.30	4.02	321	48	3	triangle
15	5.30	4.55	312	48	3	triangle
16	5.71	6.15	313	48	3	triangle
17	5.72	19.93	55	24	2	ss, 5th shell
18	5.94	4.83	512	48	3	triangle
19	5.94	5.31	251	48	3	triangle
20	6.05	4.83	431	96	3	triangle

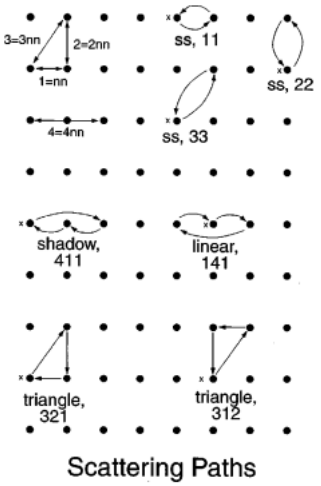

FIG. 18. Possible scattering paths in the (110) plane of an fcc lattice. The upper left corner of the figure shows the relationship between atom distances and near-neighbor distances (nn=near neighbor). The labels ss, shadow, linear, and triangle are the same path descriptions that are referred to in Table I. In particular, ss stands for single scattering. Comparing the descriptions with the actual path should make evident why these descriptions were chosen. The labels such as 11, 411, etc., are Lee and Pendry's notation (Lee and Pendry, 1975). They essentially give the near-neighbor distance of each leg in the path. The distances between atoms in the horizontal direction are 0.707 that of the distance between atoms in the vertical direction (the cube-edge distance). For this (110) plane of atoms, along the horizontal direction one has, successively, a corner atom, an atom in the center of a face, and then the next corner atom diagonal to the first, and so on. Some curved arrows were used to make the paths clearer; without them, some of the arrows would overlap each other and hence obscure each other.

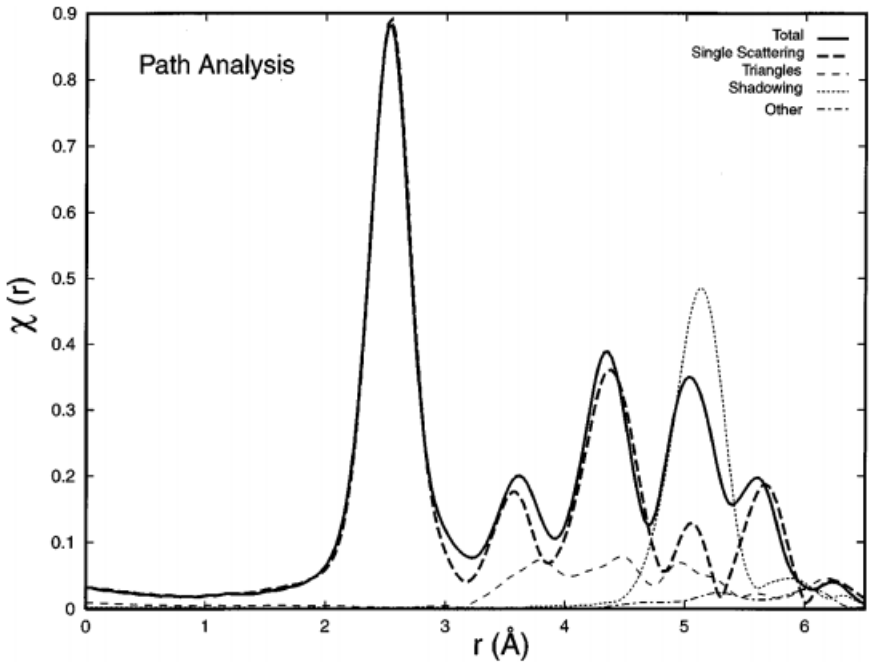

FIG. 19. Contributions of different types of multiple-scattering paths to $\chi(k)$ for Cu. Single-scattering paths are those that go from the central atom to another atom and then scatter back to the central atom. Triangular paths are those for which the path starts at the central atom, hits two other atoms, and then returns to the central atom. Shadowing paths are those for which a path starts at a central atom, hits another atom, and then goes straight through (in exactly the same direction) to hit another atom, before returning through the previous atom to the central atom. Because the forward scattering amplitude is large, shadowing paths can be accentuated by this "focusing" effect. The curve labeled "total" is the sum over all paths. The absolute values of each contribution are plotted. Because phase information is not retained in the figure, destructive interference between some of the contributions can reduce the absolute value of the total below the absolute value of some of the contributions. See also Fig. 3 of Zabinsky *et al.* (1995) for a similar figure.

2 Literature summary

- K edge = 1s
- L edge = 2s, 2p
- M edge = 3s, 3p, 3d

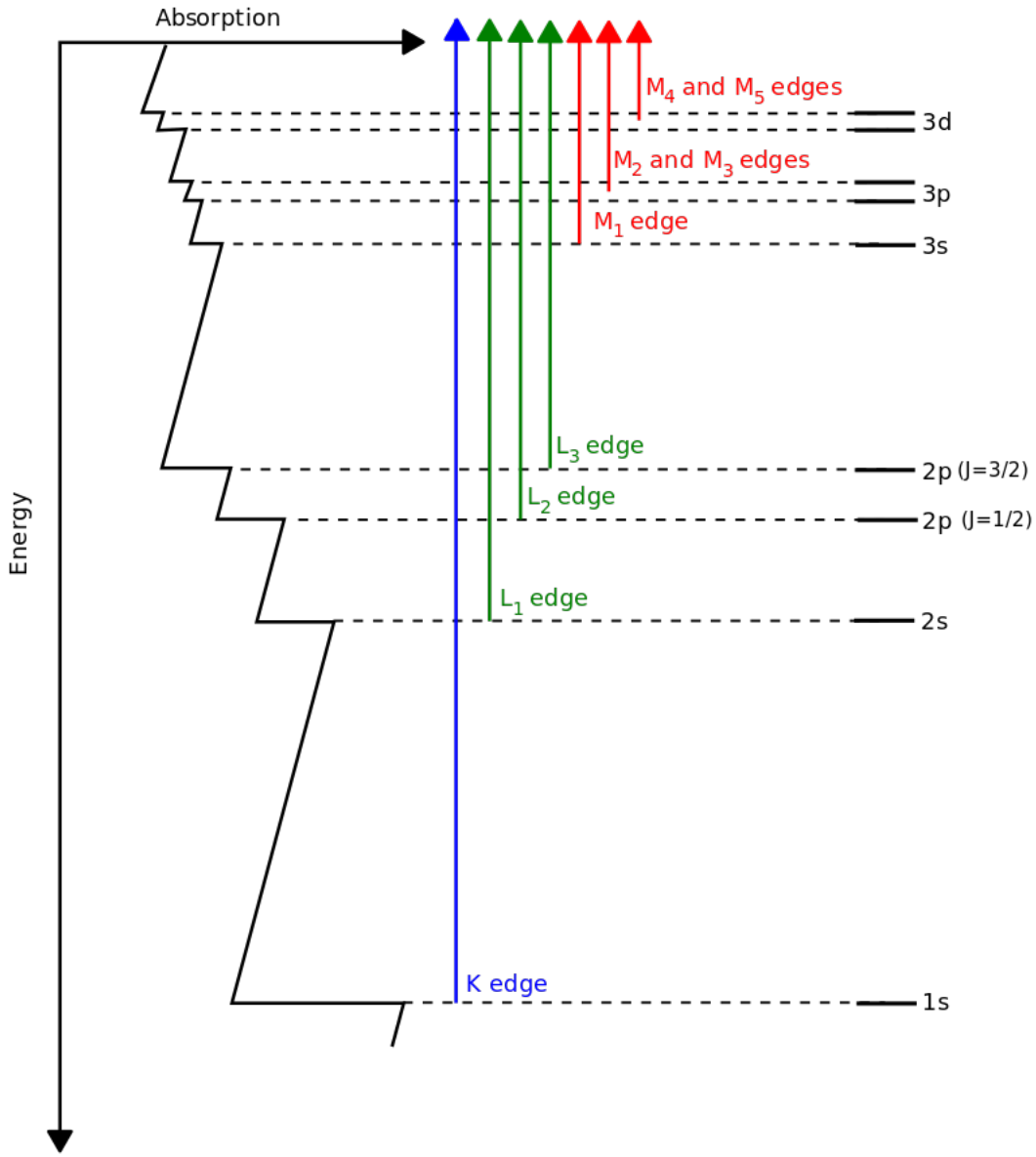

2.1 Articles from Deyu Lu

2.1.1 (Science, 2020) "Kinetic pathways of ionic transport in fast-charging lithium titanate 10.1126/science.aax3520

- distoring structure of Li4Ti5O12 (LTO) accelerates slow ground-state Li+ migration; new opportunities for high-rate electrode materials

- fast-charging applications: electrode materials that accomodate Li continuously through solid-solution transforation (few kinetic barriers apart from Li+ ion diffusion)
- except LTO; XAS to resolve sites Li+ ions occupy in different phases of transformation
- Li K-edge EELS- occupancy of Li, high sensitivity to local environment (compared to NMR, neutron diffraction)
- low-lying Li K-edge in immediate proximity to strong plasmon excitations
- emergence of new peak (M) upon charging- thought to be rate dependent- associated with distortion if Li_16c sites (face-sharing)
- also considered configurations with higher formation energies (accessible at high current rates or large overpotential)
- Z+1 approximation for EELS; supercells with gamma point and 3x empty states than occupied states (with VASP- need see what QE does)
  - aligned main peak position to main peak of experimental spectra; convolution with Gaussian, FWHM = 1 eV to mimic instrumental broadening
  - compared to spectra using OCEAN; DFT calcs from QE
  - electron-core hole interaction treated using BSE; 1600 bands (~100 eV above Fermi level) in OCEAN
  - in OCEAN, reference Li 1s core hole energy set to 8.54; also calculated relative core level shifts
  - all OCEAN spectra shifted to align with experimental spectra and broadened with 1.2 eV
  - VASP (Z+1) compared to OCEAN (BSE)oc
- barriers calculated with NEB method- stitched a series of hops in end and intermediate Li concentration structures- resulted in symmetrically equivalent beginning and end configurations for percolating pathway

2.1.2 (Nano Lett, 2019) "Ultrathin Amorphous Titania on nanowires: optimization of conformal growth and elucidation of atomic-scale motifs" 10.1021/acs.nanolett.8b04888

- analysis of glassy TiO2 polymorphs deposited on ZnO nanowires, 2-3 nm thick, conformal layers of TiO2
- first-principles analysis -> 50% undercoordinated Ti sites
- corroborate processing with XPS, XRD

- "splitting is a clear signature for at least intermediate range order in the sample"
- two approaches
  - simulated annealing procedure (VASP) to model structure amorphous TiO2;
    - 108-atoms, Verlet algorithm, Nose-Hoover;
    - 4000K equil for 1ps at 0.5 fs timestep
    - cool to 2500K at 125K/ps, equilibrilate for 2 ps
    - cool to 0K at 125 K/ps while equilibrilating for 2 ps at 500 K intervals
    - XSpectra: ecut 40 Ry (320 Ry augmented charge densities), SCF gamma points, 2x2x2 MP grid for XANES; use adsorption onset of spectra
    - OCEAN:
      - crystal rutile, anatase: 120 Ry ecut, 6x6x4 BZ sapling, 976 empty bands (340 eV above Fermi level) for final-state wavefunctions and 300 empty bands (150 eV above Fermi level) for screend core-hole
      - amorphous structure: empty bands 35 eV above Fermi level for final state, 80 eV above fermi level for screened-hole, Gamma point sampling BZ
    - relative absorption energy onset from different Ti sites in same unit cell aligned to core energy level in linear response method
  - fitting to reference spectra- ok for polyphase sample with micro- or nano-crystalline content
  - compare and contrast XSpectra (core-hole psuedopotential) and OCEAN (BSE) methods
  - use Materials Project ot build database of polymorphs, with XSPECTRA
- energy alignment procedure for XSpectra calculations (cited Ref. 16: "On the hydration and hydrolysis of carbon dioxide" Chemical Physics Letters 10.1016/j.cplett.2011.08.063):
  - energy reference in DFT is necessarily determined by the mathematical requirement that the potential in each repeated cell must average to zero
  - shift energy scale of computed DFT eigenvalues such that relative energies between different systems are meaningful; and to get alignment with experimental reference

$$E \rightarrow E - \varepsilon_{N+1}^{XCH}(i) + \Delta E_{atomic}^{C}(i) + \Delta_{exp}$$

where for configuration i, the $(N+1)$th eigenvalue of the lowest energy core-excited state (i.e., KS eigenvalue of first available state the excited electron can occupy above existing N valence elements); the relative excitation energy with respect to an isolated C atom (this study was doing hydration/hydrolysis of CO2) is caluclated using DFT total energy differences of the total system and the isolated atom in ground and excited states

$$\Delta E^{C}_{atomic}(i) = [E^{XCH}_{tot}(i) - E^{XCH}_{C}(i)] - [E^{GS}_{tot}(i) - E^{GS}_{C}(i)]$$

- energy alignment (EELS) 10.1103/PhysRevLett.89.126404
  - modern DFT calculations used in the total-energy-differences mode can predict EELS cord threshold energies with absolute energy accurage of order 1 eV
  - accomplished with pseudopotentials + atomic all-electron calculations
  - experimental standpoint- measure absolute binding energy requires long-term instrumental stability 1ppm; instead use relative core level shifts (CLS) relative to known reference
  - general theme of paper: identify where relative errors in CLS small, even it absolute binding energy sucks
  - Z+1 effective core-hole approximation in pseudopotential
  - Born-Haber cycles to infer core excitation energies; core exciton energy

    $$\Delta E^{CEX} = E^{PPX} - E^{PP0} - \Delta E^{PPA} + \Delta E^{AEA}$$

    where E^{PPX}, E^{PP0} are total energies of excited and ground states, $\Delta E^{PPA}, \Delta E^{AEA}$ are the excitation energies of the psuedopotential atoms and all-electron atoms from total energy differences
  - GGA better tha nLDA in tests onisolated atoms
  - use supercells instead of primitive cells to avoid systematic errors in substraction of large energies
  - polarization effects large for O K-edge but not for Si L3 edge

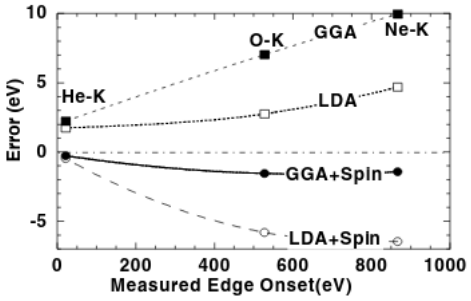

FIG. 1. Errors (with respect to the experimental measurements [21,22]) for EELS K-edge onsets ($1s \rightarrow np$) in free atoms calculated from total-energy differences within the LDA and GGA approximations, both with and without spin polarization.

– all-electron atom calculations are scalar relativistic- core excitation energy representes weighted average over spin-orbit split components; Si 2p spin orbit split is 0.61 eV

2.2 Articles based on search of David Prendergast (LBNL)

Noteworthy references: J. Stöhr, "NEXAFS Spectroscopy." Springer. 1992

2.2.1 (PRL, 2006) X-ray absorption spectra of water from first-principles calculations 10.1103/PhysRevLett.96.215502

- x-ray absorption cross section, first order using Fermi's golden rule

$$\sigma(\omega) = 4\pi^2 \alpha_0 \hbar\omega \sum_f |M_{i\rightarrow f}|^2 \delta(E_f - E_i - \hbar\omega)$$

where α_0 is fine structure constant. Matrix elements evaluated with electric-dipole approximation

$$M_{i\rightarrow f} = \langle \Psi_f | \hat{\epsilon} \cdot \mathbf{R} | \Psi_f \rangle \approx S \langle \psi_f | \hat{\epsilon} \cdot \mathbf{r} | \psi_i \rangle$$

where $\hat{\epsilon}$ is the polarization direction of electromagnetic vector potential, **R**and **r**are many-body and single-electron position operators.

- Initial state is fixed as 1s eigenstate of oxygen atom; assume S is constant for all transitions; cites Mahan here
- Final state is calculated in the presence of core-hole (due to x-ray excitation) and structure is relaxed with this constraint
- X-ray excited electron occupy only first available empty band
- Model x-ray excited atom with pseudopotential of oxygen atom with one electron removed from 1s level

- Not include breaking of spin degeneracy with single-electron excitation
- Use frozen core approximation for calculating $M_{i\to f}$;PBE GGA, QE, 85 Ry
- XCH (excited core-hole) approach; versus full core hole (FCH) and half core hole, (HCH)
  - FCH: does not include self-consistent inclusion of excited electron; should accurately reproduce higher energy excitations to progressively more delocalized states and be equivalent to XCH at high energies; tends to overestimate $\sigma(\omega)$ at/near onset, underestimately main peak height
  - HCH: half electron removed from core state- simulate transition state in x-ray excitation process
    - almost no impact on calculated XAS for water and ice
    - tends to overestimate main peak and underestimate exictonic near-edge intensity; consistent with reduced binding energy of half-core hole in excited oxygen atom
- same trends of oxygen lattice disorder and broken hydrogen bonds for all methods; in limit of converged k-point sampling and employing homogeneous numerical broadenings, XCH most consistent with experiment

2.3 Articles surrouding QE XSPECTRA

2.3.1 (PRB, 2002) First principles calculations of X-ray absorption near-edge structure calculations with the pseudopotentials: application to the K-edge in diamon and alpha-quartz 10.1103/PhysRevB.66.195107

- reciprocal-space pseudopotential for XANES; recursive method to compute absorption cross-section as continued fraction
- core-hole interaction via large supercells (100s atoms)
- XANES: medium range order of atomic arrangements of probed atom (~8 Ang)
- choice of method depends on if final state is localized or delocalized
  - localized states: crystal field multiplet theory ($L_{2,3}$ for transition metal, $M_{4,5}$ for rare-earth elements); not sure if the elements are specific or if people just haven't done other cases
  - delocalized states: multielectronic interactions are weak and single-electron DFT is good (K, L_1)

    * real-space (cluster) approach: extensive use, but drawback is muffin-tin potential approximation, requires significant computing power in certain methods, restricted to ~50 atoms w/o symmetry
    * reciprocal-space (band structure) approach: LDOS to interpret XANES; radial matrix elements to calculate XANES (WIEN2K)/ELNES (CASTEP)
        · construct all electron wave function from PAW; include excited atom in supercell
        · two-particle Bethe-Salpeter approach can be simplified to single-particle calculation because core hole is frozen at one atomic site
        · computation of cross section is limited by diagonalization of Hamiltonian for several empty states at many k-points

- main purpose of paper: incorporate faster recursion method (of Haydock, Heine, Kelly) to make supercells tractable

- In single-electron approach

$$\sigma(\omega) = 4\pi^2\alpha_0\hbar\omega \sum_f |M_{i\to f}|^2 \delta(E_f - E_i - \hbar\omega)$$

- PAW formalism, extract all electron wavefunction $|\psi_f\rangle$ from pseudowave functions $|\widetilde{\psi}_f\rangle$ via linear operator $\mathcal{T}$:

$$|\psi_f\rangle = \mathcal{T}|\widetilde{\psi}_f\rangle$$

$$\mathcal{T} = \mathbf{1} + \sum_{\mathbf{R},n} \left[|\phi_{\mathbf{R},n}\rangle - |\widetilde{\phi}_{\mathbf{R},n}\rangle\right] \langle\widetilde{p}_{\mathbf{R},n}|$$

where $n = (l, m)$ are angular momentum numbers, $|\phi_{\mathbf{R},n}\rangle$ and $|\widetilde{\phi}_{\mathbf{R},n}\rangle$ are all electron and pseudo partial waves, which coincide ouside $\Omega_{\mathbf{R}}$. $\langle\widetilde{p}_{\mathbf{R},n}|$ are called projector functions, equal to zero outside $\Omega_{\mathbf{R}}$ and satisfy $\langle\widetilde{p}_{\mathbf{R},n}|\phi_{\mathbf{R}',n'}\rangle = \delta_{\mathbf{R}\mathbf{R}'}\delta_{nn'}$.

- The $|\phi_{\mathbf{R},n}\rangle$ form a complete basis for any physical non-core all-electron wavefunction within $\Omega_{\mathbf{R}}$; thus, $|\widetilde{\phi}_{\mathbf{R},n}\rangle$ also forms a complete basis set for all physical non-core pseudo wavefunction within $\Omega_{\mathbf{R}}$. This entails for any function $\langle\mathbf{r}|\chi_{\mathbf{R}}\rangle$ centered on atomic site $\mathbf{R}$and equal to zero outside $\Omega_{\mathbf{R}}$:

$$\sum_n \langle\widetilde{\psi}|\widetilde{p}_{\mathbf{R},n}\rangle\langle\widetilde{\phi}_{\mathbf{R},n}|\chi_{\mathbf{R}}\rangle = \langle\widetilde{\psi}|\chi_{\mathbf{R}}\rangle$$

Can then rewrite the matrix elements (in terms of all electron wavefunctions) $M_{i\to f} = \langle\psi_f|\mathcal{D}|\psi_i\rangle$

$$M_{i\to f} = \langle\widetilde{\psi}_f|\mathcal{D}|\psi_i\rangle + \sum_{\mathbf{R},n}\langle\widetilde{\psi}|\widetilde{p}_{\mathbf{R},n}\rangle\langle\phi_{\mathbf{R},n}|\mathcal{D}|\psi_i\rangle - \sum_{\mathbf{R},n}\langle\widetilde{\psi}|\widetilde{p}_{\mathbf{R},n}\rangle\langle\widetilde{\phi}_{\mathbf{R},n}|\mathcal{D}|\psi_i\rangle$$

$$= \langle\widetilde{\psi}_f|\mathcal{D}|\psi_i\rangle + \sum_{\mathbf{R},n}\langle\widetilde{\psi}|\widetilde{p}_{\mathbf{R},n}\rangle\langle\phi_{\mathbf{R},n}|\mathcal{D}|\psi_i\rangle - \sum_{\mathbf{R}}\langle\widetilde{\psi}|\mathcal{D}|\psi_i\rangle$$

The initial wavefunction $\langle\mathbf{r}|\psi_i\rangle$ is localized on the absorbing atom $\mathbf{R}_0$ so only $\mathbf{R}_0$ needs to be considered. Also notice that $\langle\mathbf{r}|\mathcal{D}|\psi_i\rangle$ is zero outside $\Omega_{\mathbf{R}_0}$, which let's us invoke the relation from complete basis above- so third term vanishes (and first term also vanishes), reducing the transition amplitude $M_{i\to f}$to one term. We now define

$$|\widetilde{\varphi}_{\mathbf{R}_0}\rangle \equiv \sum_n |\widetilde{p}_{\mathbf{R}_0,n}\rangle\langle\phi_{\mathbf{R}_0}|\mathcal{D}|\psi_i\rangle$$

We can now rewrite for the x-ray absorption cross-section

$$\sigma(\omega) = 4\pi^2\alpha_0\hbar\omega\sum_f |\langle\widetilde{\psi}_f|\widetilde{\varphi}_{\mathbf{R}_0}\rangle|^2\delta(E_f - E_i - \hbar\omega)$$

Next show how recursion method can rewrite above equation as a continued fraction and avoid the calculation of empty states.

- Recursion method: for Hermitian matrix to tridiagonal form from Haydock, Heine, and Kelly. For simplicity, assume norm of all electron partial waves ϕ coincides with $\widetilde{\phi}$
  - introduce Green operator via substitution of

$$\sum_f |\widetilde{\psi}_f\rangle\delta(E_f - E_i - \hbar\omega)\langle\widetilde{\psi}_f| \to -\frac{1}{\pi}Im[\widetilde{G}(E)]$$

$$\widetilde{G}(E) = (E - \widetilde{H} + i\gamma)^{-1}$$

  - Green operator is associated with pseudo-Hamiltonian $\widetilde{H} = \mathcal{T}^\dagger H\mathcal{T}$,which is also Hermitian, $E = E_i + \hbar\omega$

- rewrite x-ray absorption cross section again (and using the fact that $|\langle\widetilde{\psi}_f|\widetilde{\varphi}_{\mathbf{R}_0}\rangle|^2 = \langle\widetilde{\varphi}_{\mathbf{R}_0}|\widetilde{\psi}_f\rangle\langle\widetilde{\psi}_f|\widetilde{\varphi}_{\mathbf{R}_0}\rangle$)

$$\sigma(\omega) = -4\pi\alpha_0\hbar\omega Im\left[\langle\widetilde{\varphi}_{\mathbf{R}_0}|(E - \widetilde{H} + i\gamma)^{-1}|\widetilde{\varphi}_{\mathbf{R}_0}\rangle\right]$$

- following Lanczos, you get $\widetilde{H}$with tridiagonal representation, which can get you matrix elements $\langle\widetilde{\varphi}_{\mathbf{R}_0}|(E - \widetilde{H} + i\gamma)^{-1}|\widetilde{\varphi}_{\mathbf{R}_0}\rangle$ with low cost

- this new Lanczos basis is obtained by repeated action of $\widetilde{H}$ on some random initial vector $|u_0\rangle = |\widetilde{\varphi}_{\mathbf{R}_0}\rangle / \sqrt{\langle \widetilde{\varphi}_{\mathbf{R}_0} | \widetilde{\varphi}_{\mathbf{R}_0} \rangle}$ through the symmetric three-term recurrence relation

$$\widetilde{H}|u_i\rangle = a_i|u_i\rangle + b_{i+1}|u_{i+1}\rangle + b_i|u_{i-1}\rangle$$

where $a_i = \langle u_i \widetilde{H} | u_i \rangle$ and $b_i = \langle u_i | \widetilde{H} | u_{i-1} \rangle = \langle u_{i-1} | \widetilde{H} | u_i \rangle$ are real parameters

- rewrite the matrix elements the tridiagonal matrix of $\widetilde{H}$ in the $\{|u_i\rangle\}$basis in a continued fraction

$$\langle \widetilde{\varphi}_{\mathbf{R}_0} | (E - \widetilde{H} + i\gamma)^{-1} | \widetilde{\varphi}_{\mathbf{R}_0} \rangle = \cfrac{\langle \widetilde{\varphi}_{\mathbf{R}_0} | \widetilde{\varphi}_{\mathbf{R}_0} \rangle}{a_0 - E - i\gamma - \cfrac{b_1^2}{a_1 - E - i\gamma - \cfrac{b_2^2}{\ddots}}}$$

- terminate continued fraction: implemented simple condition, i.e., for N iterations to converge calculation, consider (a_i, b_i) are equal to (a_N, b_N) for $i > N$
- number iterations N strongly depends on broadening parameter γ
- overall, the main part of the XANES calculation involves computation of Hamiltonian acting on single vector- much faster
- Comparison with Bethe-Salpeter approach (of other studies)
  - this study uses DFT energies, which is no problem if GW results in rigid shift
  - this study screens core hole by valence electrons at all orders computed self-consistently in DFT
  - core hole and electron interaction in final state approximated with LDA
  - (more methodological difference than fundamental) use plane-wave basis of supercell
- Basic steps to applications
  - evalutate self-consistent charge density for supercells including one 1s core hole
  - construct and converge $\{|u_i\rangle\}$ basis to find tridiagonal representation of pseudo-Hamiltonian
- Other calculation parameters: LDA, norm-conserving TM pseudopotentials; the excited atom has pseudopotential with only one 1s electron - somehow this is generated;

- Test case: carbon K-edge of diamond
  - spectra converged up to 250 atoms
  - separate k-point convergence for charge density and Lanczos; Lanczos grid requires much larger, on the scale of a DOS calculation (even for supercells)
  - $\gamma = 0.3$ eV; number of $|u_i\rangle \sim 800 - 1400$, worded in a way that makes it seem more are needed with larger supercell size
  - first 4 eV of spectrum not reproduced well in calculations- missing exciton peak and interaction of core-holes b/t periodic images; supercell size greatest impact on first couple eV, which conversely gives info on the volume seen by photoelectron during absorption process; for diamond, this is ~6 Ang radius
  - FEFF8: muffin-tin, 300 atom cluster, neglects core-hole effects, which seem to be important for diamond at least
- Test case: silicon and oxygen K-edge of α-quartz
  - compare with polarized K-XANES experiments; α-quartz is dichroic, so absorption spectrum is linear combination of $\sigma_{\parallel}$and $\sigma_{\perp}$- so need to look into angular dependence of absorption
  - here only need supercells of 72 atoms; smaller k-point grid for charge density and Lanczos; $\gamma = 1$eV for $|u_i\rangle \sim 500 - 600$
  - core-hole is super important to capture peaks in first few eV of spectra

2.3.2 (PRB,2009) Intrinsic charge transfer gap in NiO from Ni K-edge x-ray absorption spectroscopy 10.1103/PhysRevB.79.045118

- K-edge XAS difficult because excitations occur in large energy window above Fermi level; most methods dealing with correlation for states close to Fermi level
- need to describe correlations at high energy levels: 1) low-energy pre-edge features $\rightarrow$ local environment of absorbing atom, 2) correlated oxides "shakedown" excitations occur as near-edge structure
- implementation with DFT+U(=7.6 eV), U from linear response (Kulik); PAWs
- pre-edge dipolar feature in Ni K-edge XAS from nonlocal excitations to second NN Ni atoms; unshifted by core-hole attraction and is a simple/reliable measure of upper Hubbard band in the absence of a core hole in the final state; insensitivity of pre-edge dipolar feature to core-hole attraction means can directly measure charge transfer gap using K-edge XAS
  - $\epsilon \parallel [110]$, $\mathbf{k} \parallel [-110] \rightarrow e_g$ orientation

  - $\epsilon \parallel [100]$, $\mathbf{k} \parallel [010] \rightarrow t_{2g}$ orientation; no quadrupolar transition

- U has little effect on high-energy near-edge and far-edge features (> 10 eV); but noticeable effect of features < 10 eV
- align zero of XANES to Fermi level in presence of core hole and use pDOS to show contributions from absorbing Ni, nearest-neighbor Ni, and second nearest-neighbor Ni (and O atoms)
- experiments with partial fluorescence yield?
- core-hole attraction can substantially lower d states

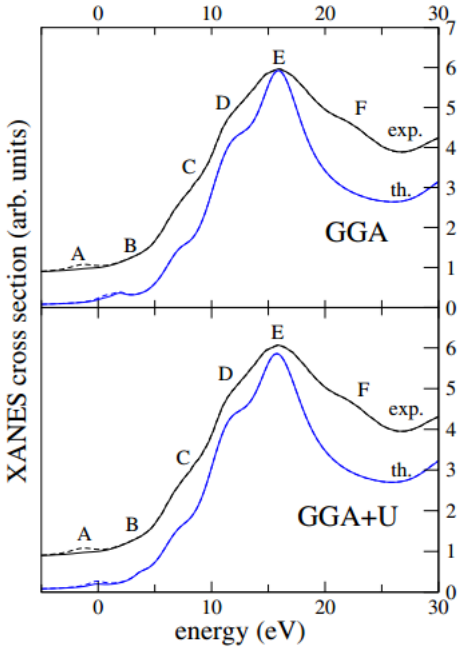

FIG. 1. (Color online) Calculated and measured (Ref. 23) Ni K-edge XAS of NiO. The dashed (solid) curves correspond to e_g (t_{2g}) orientation.

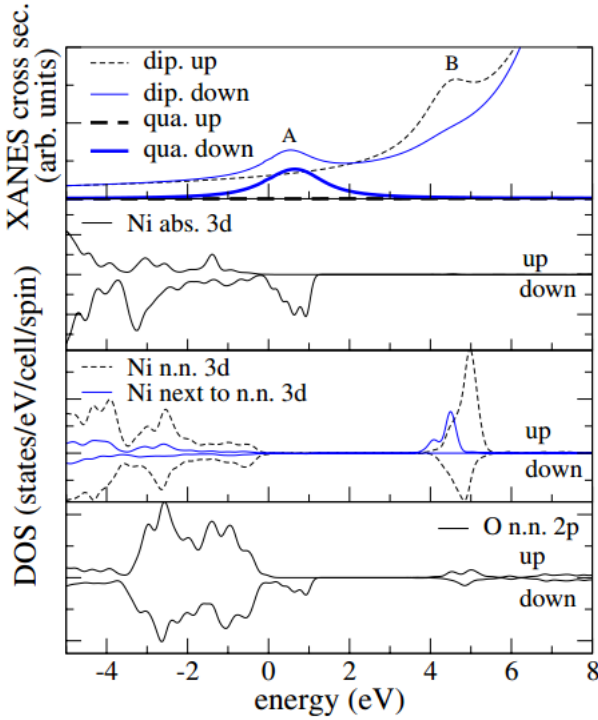

FIG. 3. (Color online) Comparison between GGA+U calcul
K-edge Ni XAS and Löwdin projected density of states.

- interpretation of peaks
  - peak A: quadrupolar, intrasite excitations to d states lowered by core-hole attraction, which also lowers small portion of O 2p states (b/c Ni and O hybridization is strong)
    - atomic picture: Ni $1s \rightarrow$ O$2p$
  - peak B: transitions to up-spin-polarized states; dipolar; excitation must be offsite b/c absorbing Ni has 5 up d electrons; transitions to

onsite hybridized Ni $4p-3d$ states to empty $3d$ states of second NN Ni; nonlocal!

  * intersite Ni $4p-3d$ mixing via strong Ni $3d-$O$2p$ hybridization
  * direct probe of upper Hubbard band in NiO- don't really understand this part of the argument

- physical interpretation of Hubbard term role: U reduces hybridization of Ni $3d$ and O $2p$ states via larger occupation of Ni $3d$ states and consequent energy shift down, which raises empty Ni $3d$ states
- peak shifts on the order of ~4 eV comparing GGA and GGA+U
- measuring charge transfer gap (aka "correlation gap") with hole doped NiO (e.g., Li-doping)
  - holes mainly on O so expect additional dipolar peak in pre-edge
  - hole doping calculated with 2 methods: 1) rigid-band doping, 2) adding compensating-charge background and recalculating self-consistent charge density and XAS
  - rigid doping is a pretty good approximation to compensating-charge background for low doping ($0 < x < 0.2$, $\mathrm{Li}_x\mathrm{Ni}_{1-x}\mathrm{O}$); as usual, small energy pre-edge features disagree the most
  - in the absence of core-hole effects, peak B measures correlation gap (5 eV); optical absorption onset at 3.1 eV (lower due to excitons-man, that's a lot of excitons)
  - applicable to other charge transfer insulators

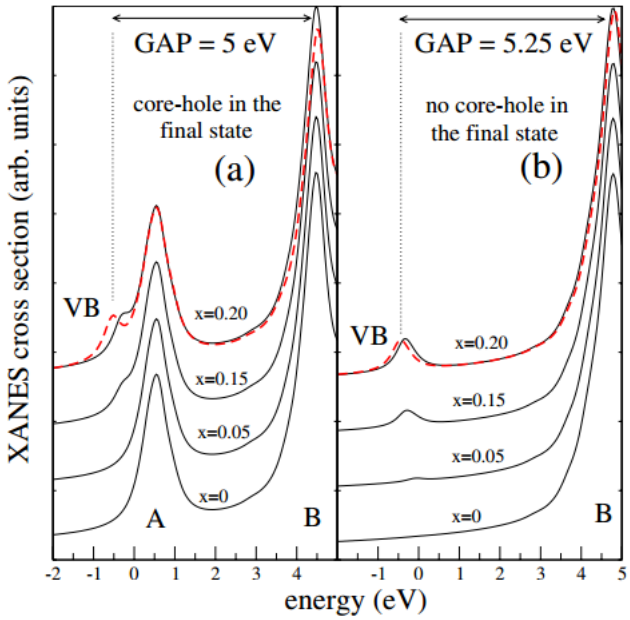

FIG. 5. (Color online) Calculated pre-edge features of Ni *K*-edge XAS spectra of $Li_xNi_{1-x}O$ with (a) and without (b) core-hole effects using a rigid doping (solid line) approach or adding a compensating-charge background (red dashed lines). Peak labeling is the same as in Fig. 1; VB stands for valence band.

2.3.3 (PRB, 2009) First-principles calculations of x-ray absorption in a scheme based on ultrasoft pseudopotentials 10.1103/PhysRevB.80.075102

3 Relating to algorithms

3.1 Lanczos procedure

3.1.1 C. Lanczos "Solutions of Systems of linear equation by minimized iterations" link

- method that is well-adapted to the effective solution of large systems of linear algebraic equations by a succession of well-convergence approximations (1 sentence abstract; baller)